Influences of porosity and tangential edge constraint on thermo-torsional postbuckling of FGM toroidal shell segments surrounded by an elastic medium

L. T. NHU TRANG[1)], H. VAN TUNG[2)]

[1)] *Faculty of Civil Engineering, University of Transport Technology, 54, Trieu Khuc, Thanh Xuan, Ha Noi, Viet Nam*

[2)] *Faculty of Civil Engineering, Hanoi Architectural University, Km 10, Nguyen Trai, Thanh Xuan, Ha Noi, Viet Nam,*
e-mails: tunghv@hau.edu.vn, hoangtung0105@gmail.com (corresponding author)

For the first time, simultaneous influences of porosities, tangential constraints of boundary edges, surrounding elastic media and elevated temperature on the buckling and postbuckling behaviors of a functionally graded toroidal shell segment are investigated in this paper. Porosities exist in the functionally graded material (FGM) according to even and uneven distributions. Properties of constituent materials are assumed to be temperature dependent and effective properties of the porous FGM are determined using a modified rule of mixture. Governing equations are based on the classical shell theory taking into account geometrical nonlinearity and interactive pressure from surrounding elastic medium. Multi-term analytical solutions are assumed to satisfy simply supported boundary conditions and the Galerkin method is adopted to derive nonlinear load – deflection relations and buckling loads. Parametric studies are carried out to analyze the effects of porosity, shell geometry, degree of tangential edge constraint, elevated temperature and elastic media on the buckling resistance and postbuckling strength of toroidal shell segments under a torsional load. The study reveals that tangential edge restraints have considerably beneficial and detrimental influences on the nonlinear stability of torsion-loaded FGM shells at room and elevated temperatures, respectively. The results also find out that the shear layer and the elastic layer of surrounding medium significantly enhances and alleviates the buckling resistance capacity and severity of the snap-through response of the torsion-loaded porous FGM toroidal shell segment, respectively.

Key words: nonlinear buckling, porous FGM, toroidal shell segment, tangential edge constraint, torsional load.

1. Introduction

Due to advanced properties, the functionally graded material (FGM) is widely used in many various fields, especially in structural components. Shen [1, 2] used the classical shell theory (CST) and asymptotic solutions to investigate the postbuckling behavior of the circular cylindrical shell

(CCS) made of FGM and subjected to axial compression and external pressure in thermal environments. The buckling problem of thin FGM CCSs under thermal loads was dealt with by Wan and Li [3] employing the CST and shooting methods. Basing on an analytical approach and the CST, Tung and Hieu [4, 5] studied the buckling and postbuckling of FGM CCSs loaded by axial compression, external pressure and a uniform temperature rise. Thermal buckling and postbuckling analyses of FGM plates and cylindrical shells have been performed by Trabelsi *et al.* [6, 7] making use of a modified version of the first order shear deformation theory (FSDT) and the finite element method. Employing the higher order shear deformation theory (HSDT) and an adjacent equilibrium criterion, Bagherizadeh *et al.* [8] carried out a linear buckling analysis for FGM CCSs surrounded by an elastic medium and subjected to combined mechanical loads. The effects of surrounding elastic media on postbuckling of axially loaded FGM CCSs are analyzed in work of Shen [9] using the HSDT and asymptotic solutions. Foroutan and Dai [10] presented a semi-analytical investigation on thermal post-buckling of imperfect sigmoid functionally graded shells in thermal environment.

Pores can exist in the FGM in the manufacturing process and influence the properties of this composite. Accordingly, the assessment of effects of porosity on the response of FGM structures should be addressed. Linear and nonlinear vibration analyses of FGM beams with porosity and elastically restrained ends were performed in work [11] using the differential transformation method. The influence of porosity on the linear stability of FGM plates was examined by Gupta and Talha [12] utilizing a numerical approach. Using an analytical solution, Cong *et al.* [13] explored the postbuckling behavior of porous FGM plates under axial compression in thermal environments. Trinh *et al.* [14] employed a semi-analytical approach for a stochastic buckling analysis of FGM plates with porosities. Based on HSDT and isogeometric approaches, Cuong *et al.* [15] dealt with a nonlinear stability problem of FGM microplates with porosities under thermal loads. Analytical investigations on nonlinear stability of FGM CCSs, circular plates and spherical caps with porosities and elastically restrained edges have been performed by Long and Tung [16–18].

The stability of CCSs under torsional loads is a problem of considerable importance. Studies on buckling of laminated composite and orthotropic CCSs under torsion were addressed in works [19, 20] employing shear deformation theories. The influences of imperfection on buckling and postbuckling of isotropic CCSs under a torsional load are analyzed in work of Zhang and Han [21]. Using an analytical approach, Sofiyev and coworkers [22, 23] presented results for vibrational and buckling analyses of the FGM, orthotropic and sandwich CCSs surrounded by an elastic medium and subjected to torsion. Making use of the HSDT and a singular perturbation technique, Shen [24, 25] investigated the

buckling and postbuckling behaviors of the FGM and carbon nanotube reinforced composite (CNTRC) CCSs subjected to torsional loads in thermal environments. Basing on CST, HUANG and HAN [26] explored the buckling and postbuckling of thin FGM CCSs under torsion. A buckling analysis of FGM CCSs under the combined action of external pressure, axial compression and torsion has been carried out by HUANG *et al.* [27] using the Ritz energy and finite element methods. The effects of eccentric stiffeners and surrounding elastic media on torsional buckling and postbuckling of FGM CCSs were addressed in works of DUNG and HOA [28, 29] and NAM *et al.* [30, 31].

The toroidal shell segment (TSS) is a circumferentially closed and doubly curved shell widely used in many fields, especially in aerospace structures and pressure vessels. Nevertheless, due to complexity of shell geometry, investigations on these shells are much fewer than studies on beams, plates and panels. Some studies on buckling and postbuckling of isotropic TSSs under mechanical loads have been addressed in works [32–34] using analytical solutions. NINH and BICH [35] used the CST and an analytical approach to dealt with the buckling and postbuckling behaviors of eccentrically stiffened thin FGM TSSs surrounded by an elastic medium and subjected to torsional loads. Using the HSDT and two-term deflection solution, LONG and TUNG [36, 37] studied the buckling behavior of thick FGM TSSs with porosities under axial compression, external pressure and elevated temperature. The influences of surrounding elastic medium and tangential constraints of edges on the stability of thin and moderately thick carbon nanotube reinforced composite TSSs under external pressure and thermal load have been assessed in works of HIEU and TUNG [38, 39]. Recently, TRANG and TUNG have investigated the postbuckling behavior of functionally graded porous TSSs with tangentially restrained edges under a uniform temperature rise [41] and with movable edges under the combined action of external pressure and axial compression [42]. Previous studies [37–40] indicated that elasticity of tangential edge constraints dramatically affect the buckling and postbuckling behaviors of the porous FGM and nanocomposite TSSs subjected to elevated temperature, lateral pressure and the combined action of lateral pressure and axial compression. Nevertheless, the postbuckling problem of porous FGM TSSs surrounded by an elastic medium, exposed to a thermal environment and subjected to torsional load has not been addressed. This evident deficiency motivates the present work.

Two expected trends of nonlinear stability behavior of closed shells are that critical loads are large and snapping jumps are benign. In other words, it is expected that buckling loads and postbuckling equilibrium paths of the shell are high and stable, respectively. It is essential to assess numerous effects on the nonlinear stability of FGM TSSs with porosity under torsion. In the present paper, for the first time, simultaneous influences of porosity, tangential edge con-

straints, surrounding elastic medium and elevated temperature on the buckling and postbuckling behaviors of FGM TSSs under torsional load are investigated. The porosities are distributed in FGM according to even and uneven patterns and effective properties of FGM are determined using a modified rule of mixture. Governing equations for a nonlinear stability problem are established within the framework of the classical shell theory taking into consideration geometrical non-linearity and interactive pressure from surrounding elastic medium. Multi-term analytical solutions are assumed to satisfy simply supported boundary conditions and the Galerkin method is used to derive nonlinear relation between load and deflection. Parametric studies are carried out and the novel findings are obtained.

2. Material and structural models

The structural model of the present study is a toroidal shell segment (TSS) of thickness h, length L and curvature radii in the circumferential and meridional directions R and a, respectively, as shown in Fig. 1. The TSS is surrounded by an elastic medium modelled as a two-parameter foundation. The TSS is defined in a coordinate system xyz, the origin of which is located on the middle surface, x and y are meridional and circumferential coordinates, respectively, and z is in the direction of inward normal to the mid-plane of the shell. The TSS is assumed to be very shallow in the meridional direction and, thus, R/a ratio is much smaller than unity. As a special case, TSS returns to a circular cylindrical shell when a tends to infinity.
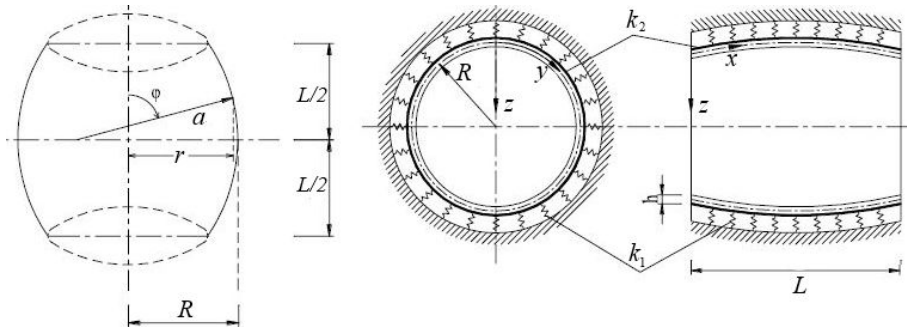

Fig. 1. Configuration and coordinate system of a toroidal shell segment (TSS) surrounded by an elastic medium.

In this study, TSS is made of ceramic-metal functionally graded material (FGM) with porosity. The volume fraction V of each constituent in FGM is assumed to vary across the thickness according to a power law function as [1, 2]

$$(2.1) \qquad V_m = \left(\frac{1}{2} + \frac{z}{h}\right)^N, \qquad V_c = 1 - V_m,$$

where $N \geq 0$ is the volume fraction index and subscripts c and m represent ceramic and metal constituents, respectively. According to Eq. 2.1, inner and outer surfaces of the TSS are metal-rich and ceramic-rich, respectively. Due to existence of pores, the effective properties P_{eff} of FGM are evaluated using a modified rule of mixture as [11]:

$$(2.2) \qquad P_{eff} = P_m\left(V_m - \frac{\xi}{2}\right) + P_c\left(V_c - \frac{\xi}{2}\right),$$

where $0 \leq \xi \ll 1$ is a very small value representing the volume fraction of porosity and P stands for a specific property of constituents. When ξ tends to zero, the FGM is without porosity and is referred to as a perfect FGM.
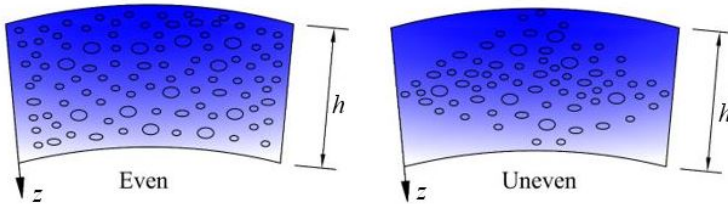

FIG. 2. Even and uneven types of porosity distribution within the shell.

In this work, porosities are assumed to distribute within the FGM according to even and uneven patterns. In even distribution pattern, porosity density at any point in the FGM is uniform. In an uneven distribution type, porosities concentrate more at region near the middle surface of the TSS, as illustrated in Fig. 2. By using Eq. (2.1) into Eq. (2.2), effective elastic modulus E and thermal expansion coefficient α of the porous FGM are determined as [11]:

$$(2.3a) \qquad E(z, T) = [E_m(T) - E_c(T)]\left(\frac{1}{2} + \frac{z}{h}\right)^N$$
$$+ E_c - \frac{\xi}{2}[E_m(T) + E_c(T)]\left(1 - 2\chi\frac{|z|}{h}\right),$$

$$(2.3b) \qquad \alpha(z, T) = [\alpha_m(T) - \alpha_c(T)]\left(\frac{1}{2} + \frac{z}{h}\right)^N$$
$$+ \alpha_c - \frac{\xi}{2}[\alpha_m(T) + \alpha_c(T)]\left(1 - 2\chi\frac{|z|}{h}\right),$$

where $\chi = 0$ and $\chi = 1$ correspond to even and uneven distributions, respectively, and dependence on temperature T of materials is included. Due to weak

dependence on temperature and position, the Poisson ratio ν of the FGM is assumed to be constant.

3. Governing equations

This study considers a specific class of TSSs that are thin and geometrically perfect TSSs. For these TSSs, transverse shear deformation is negligibly small and the classical shell theory (CST) along with the Stein–McElman assumption [32] are used for establishing basic equations. On the basis of the CST, strains at a point in the shell are expressed as follows [32, 35]:

$$(3.1) \qquad \begin{pmatrix} \varepsilon_x \\ \varepsilon_y \\ \gamma_{xy} \end{pmatrix} = \begin{pmatrix} \varepsilon_x^0 \\ \varepsilon_y^0 \\ \gamma_{xy}^0 \end{pmatrix} + z \begin{pmatrix} k_x \\ k_y \\ k_{xy} \end{pmatrix},$$

where

$$(3.2) \qquad \begin{pmatrix} \varepsilon_x^0 \\ \varepsilon_y^0 \\ \gamma_{xy}^0 \end{pmatrix} = \begin{pmatrix} u_{,x} - w/a + w_{,x}^2/2 \\ v_{,y} - w/R + w_{,y}^2/2 \\ u_{,y} + v_{,x} + w_{,x}w_{,y} \end{pmatrix}, \qquad \begin{pmatrix} k_x \\ k_y \\ k_{xy} \end{pmatrix} = - \begin{pmatrix} w_{,xx} \\ w_{,yy} \\ 2w_{,xy} \end{pmatrix},$$

where u, v are in-plane displacements in x, y directions, respectively, and w is lateral displacement (i.e. deflection) of a point on the mid-surface. As usual, a subscript comma indicates a partial derivative with respect to the followed variable, for example $w_{,x} = \partial w/\partial x$.

Stress-strain relations accounting for temperature effects are written as [1, 2]:

$$(3.3) \qquad \begin{aligned} (\sigma_x, \sigma_y) &= \frac{E}{1 - \nu^2}[(\varepsilon_x, \varepsilon_y) + \nu(\varepsilon_y, \varepsilon_x) - (1 + \nu)(1, 1)\alpha\Delta T], \\ \sigma_{xy} &= \frac{E}{2(1 + \nu)}\gamma_{xy}, \end{aligned}$$

where $\Delta T = T - T_0$ is the uniform temperature rise from a room temperature $T_0 = 300\,\mathrm{K}$ at which the TSS is assumed to be free from thermal stresses.

Force and moment resultants per a unit length are computed through the stresses as [1, 2]:

$$(3.4) \qquad \begin{aligned} (N_x, N_y, N_{xy}) &= \int\limits_{-h/2}^{h/2} (\sigma_x, \sigma_y, \sigma_{xy})\, dz, \\ (M_x, M_y, M_{xy}) &= \int\limits_{-h/2}^{h/2} (\sigma_x, \sigma_y, \sigma_{xy})z\, dz. \end{aligned}$$

By substituting Eqs. (3.1) and (3.3) into Eq. (3.4), force and moment resultants are rewritten in the form:

$$(N_x, M_x) = \frac{1}{1-\nu^2}[(E_1, E_2)(\varepsilon_x^0 + \nu\varepsilon_y^0) + (E_2, E_3)(k_x + \nu k_y)]$$
$$- \frac{1}{1-\nu}(\Phi_0, \Phi_1),$$

$$(3.5) \qquad (N_y, M_y) = \frac{1}{1-\nu^2}[(E_1, E_2)(\varepsilon_y^0 + \nu\varepsilon_x^0) + (E_2, E_3)(k_y + \nu k_x)]$$
$$- \frac{1}{1-\nu}(\Phi_0, \Phi_1),$$

$$(N_{xy}, M_{xy}) = \frac{1}{2(1+\nu)}(E_1, E_2)\gamma_{xy}^0 + \frac{1}{2(1+\nu)}(E_2, E_3)k_{xy},$$

where

$$(3.6) \qquad (E_1, E_2, E_3) = \int\limits_{-h/2}^{h/2} E(1, z, z^2)\, dz, \quad (\Phi_0, \Phi_1) = \int\limits_{-h/2}^{h/2} E\alpha\Delta T(1, z)\, dz.$$

Interactive pressure from surrounding elastic medium is represented according to the Winkler–Pasternak model as:

$$(3.7) \qquad q_f = k_1 w - k_2(w_{,xx} + w_{,yy}),$$

where k_1 and k_2 are stiffness parameters of the Winkler elastic layer and the Pasternak shear layer, respectively. By introducing a stress function $f(x, y)$ defined as $N_x = f_{,yy}$, $N_y = f_{,xx}$, $N_{xy} = -f_{,xy}$, nonlinear equilibrium equation of a FGM TSS surrounded by an elastic medium is expressed in the following form:

$$(3.8) \qquad D\nabla^4 w - f_{,yy}w_{,xx} + 2f_{,xy}w_{,xy} - f_{,xx}w_{,yy}$$
$$- \frac{f_{,xx}}{R} - \frac{f_{,yy}}{a} + k_1 w - k_2(w_{,xx} + w_{,yy}) = 0$$

in which ∇^2 and D denote the Laplace operator and flexural rigidity, respectively, as follows:

$$(3.9) \qquad \nabla^2 = \frac{\partial^2}{\partial x^2} + \frac{\partial^2}{\partial y^2}, \quad D = \frac{E_1 E_3 - E_2^2}{E_1(1 - \nu^2)}.$$

From Eqs. (3.2) and (3.5), the strain compatibility equation of a thin porous FGM TSS is written in terms of the deflection and stress function as follows [40, 41]

$$(3.10) \qquad \nabla^4 f - E_1\left(w_{,xy}^2 - w_{,xx}w_{,yy} - \frac{w_{,xx}}{R} - \frac{w_{,yy}}{a}\right) = 0.$$

Two boundary edges of TSS are assumed to be simply supported and elastically restrained in tangential displacement. Associated boundary conditions are written as follows [24]:

$$(3.11) \quad w = 0, \quad M_x = 0, \quad N_x = N_{x0}, \quad \frac{1}{2\pi Rh} \int\limits_0^{2\pi R} N_{xy}\, dy = \tau \quad \text{at } x = 0, L,$$

where τ is uniform shear stress and N_{x0} is fictitious compressive force resultant related to average end-shortening displacement as the following [5, 38]:

$$(3.12) \qquad N_{x0} = -\frac{c}{2\pi RL} \int\limits_0^{2\pi R} \int\limits_0^L \frac{\partial u}{\partial x}\, dx\, dy$$

in which c is an average tangential stiffness parameter at two boundary edges. The values of $c = 0$, $c \to \infty$ and $0 < c < \infty$ represent movable, immovable and partially movable edges, respectively.

The condition on circumferentially closed displacement of a TSS is fulfilled in an average sense as [1, 2]

$$(3.13) \qquad \int\limits_0^{2\pi R} \int\limits_0^L \frac{\partial v}{\partial y}\, dx\, dy = 0.$$

4. Solution procedure

As discussed in the work of SHEN [24], it is very difficult to obtain exact solutions describing the behavior of torsion-loaded CCS and TSS. Hence, approximate solutions may provide reasonable predictions for a preliminary design. In the present work, approximate solutions of the deflection w and the stress function f are assumed to be in the form [26, 28, 35]:

$$(4.1a) \qquad w = W_0 + W_1 \sin \beta x \sin \delta(y - \gamma x) + W_2 \sin^2 \beta x,$$

$$(4.1b) \qquad f = A_1 \cos 2\beta x + A_2 \cos 2\delta(y - \gamma x) + A_3 \cos \delta\left[y + \left(\frac{\beta}{\delta} - \gamma\right)x\right]$$

$$+ A_4 \cos \delta\left[y - \left(\frac{\beta}{\delta} + \gamma\right)x\right] + A_5 \cos \delta\left[y - \left(3\frac{\beta}{\delta} + \gamma\right)x\right]$$

$$+ A_6 \cos \delta\left[y + \left(3\frac{\beta}{\delta} - \gamma\right)x\right] - \tau hxy + \frac{1}{2}N_{x0}y^2,$$

where W_0, W_1 and W_2 are amplitudes of deflection at prebuckling, linear buckling and nonlinear buckling states, respectively, $\beta = m\pi/L$, $\delta = n/R$ with m and

n are numbers of half and full waves in the meridional and circumferential directions, respectively. Additionally, γ is the tangent of an angle between the wave shape and the x axis and A_k $(k = 1, \ldots, 6)$ are coefficients to be determined. It is noted that the last term in the stress function, i.e. $N_{x0}y^2/2$, is the novel development of the present work in comparison with previous works [26, 28, 30, 35] neglecting the tangential constraints of edges.

By introducing solutions Eqs. (4.1) into the compatibility equation Eq. (3.10), we can determine the coefficients A_k $(k = 1, \ldots, 6)$ in the stress function as:

(4.2)
$$
\begin{aligned}
A_1 &= \frac{E_1}{8\beta^2}\left(\frac{\delta^2}{4}W_1^2 - \frac{W_2}{R}\right), \qquad A_2 = \frac{E_1\beta^2}{32\delta^2(1+\gamma^2)^2}W_1^2, \\
A_3 &= \frac{E_1 W_1}{2[(\beta - \delta\gamma)^2 + \delta^2]^2}\left[\beta^2\delta^2 W_2 - \frac{1}{R}(\beta - \delta\gamma)^2 - \frac{\delta^2}{a}\right], \\
A_4 &= \frac{E_1 W_1}{2[(\beta + \delta\gamma)^2 + \delta^2]^2}\left[\frac{1}{R}(\beta + \delta\gamma)^2 + \frac{\delta^2}{a} - \beta^2\delta^2 W_2\right], \\
A_5 &= \frac{E_1\beta^2\delta^2 W_1 W_2}{2[(3\beta + \delta\gamma)^2 + \delta^2]^2}, \qquad A_6 = -\frac{E_1\beta^2\delta^2 W_1 W_2}{2[(3\beta - \delta\gamma)^2 + \delta^2]^2}.
\end{aligned}
$$

By substituting solutions Eqs. (4.1) into the equilibrium equation Eq. (3.8) and applying the Galerkin method on the whole region of the shell $(0 \leq x \leq L, 0 \leq y \leq 2\pi R)$ to the obtained equation, we receive the following results:

(4.3a) $\qquad g_{11} + g_{21}\bar{W}_1^2 + g_{31}\bar{W}_2^2 - g_{41}\bar{W}_2 + g_{51}\bar{N}_{x0} - 2\tau\gamma\dfrac{n^2}{R_h^2} = 0,$

(4.3b) $\qquad g_{02}\bar{W}_0 + g_{12}\bar{W}_1^2 - g_{22}\bar{W}_2 - g_{32}\bar{W}_1^2\bar{W}_2 + \left(\dfrac{R_a}{R_h} - g_{42}\bar{W}_2\right)\bar{N}_{x0} = 0,$

where

(4.4) $\qquad (\bar{W}_1, \bar{W}_2, \bar{N}_{x0}, R_h) = \dfrac{1}{h}(W_1, W_2, N_{x0}, R), \qquad R_a = \dfrac{R}{a},$

and coefficients g_{i1} $(i = 1, \ldots, 5)$, g_{j2} $(j = 0, \ldots, 4)$ will are displayed in Eqs. (A.1) and (A.2) in Appendix.

Next, specific expressions of $\bar{W}_0$ and $\bar{N}_{x0}$ will be determined. From Eqs. (3.2) and (3.5), we can obtain the following relations:

(4.5a) $\qquad \dfrac{\partial u}{\partial x} = \dfrac{1}{E_1}(f_{,yy} - \nu f_{,xx}) + \dfrac{E_2}{E_1}w_{,xx} - \dfrac{1}{2}w_{,x}^2 + \dfrac{w}{a} + \dfrac{\Phi_0}{E_1},$

(4.5b) $\qquad \dfrac{\partial v}{\partial y} = \dfrac{1}{E_1}(f_{,xx} - \nu f_{,yy}) + \dfrac{E_2}{E_1}w_{,yy} - \dfrac{1}{2}w_{,y}^2 + \dfrac{w}{R} + \dfrac{\Phi_0}{E_1}.$

Using the solutions Eqs. (4.1) into the above relations and putting the obtained expressions into Eqs. (3.12) and (3.13) yield the following results:

$$(4.6a) \qquad \bar{N}_{x0} = \lambda \left[g_{13}\bar{W}_1^2 + g_{23}\bar{W}_2^2 - \frac{\bar{E}_1 R_a}{2R_h}(2\bar{W}_0 + \bar{W}_2) - G\Delta T \right],$$

$$(4.6b) \qquad -\frac{\nu}{\bar{E}_1}\bar{N}_{x0} - \frac{n^2}{8R_h^2}\bar{W}_1^2 + \frac{1}{2R_h}(2\bar{W}_0 + \bar{W}_2) + \frac{G}{\bar{E}_1}\Delta T = 0,$$

where

$$(4.7) \qquad \lambda = \frac{c}{E_1 + c}, \quad g_{13} = \frac{\bar{E}_1}{8R_h^2 L_R^2}(m^2\pi^2 + \gamma^2 n^2 L_R^2),$$

$$g_{23} = \frac{\bar{E}_1 m^2 \pi^2}{4R_h^2 L_R^2}, \quad G = \frac{1}{h}\int\limits_{-h/2}^{h/2} E\alpha\,dz.$$

Solving Eqs. (4.6) for $\bar{W}_0$ and $\bar{N}_{x0}$, we receive:

$$(4.8a) \qquad \bar{W}_0 = -\frac{\bar{W}_2}{2} + d_{11}\bar{W}_1^2 + d_{21}\bar{W}_2^2 - d_{31}\Delta T,$$

$$(4.8b) \qquad \bar{N}_{x0} = \lambda(d_{12}\bar{W}_1^2 + d_{22}\bar{W}_2^2 - d_{32}\Delta T),$$

where coefficients d_{ij} ($i = 1,\ldots,3$, $j = 1,2$) are displayed in Eq. (A.4), in Appendix.

Substituting $\bar{W}_0$ and $\bar{N}_{x0}$ from Eq. (4.8) into Eq. (4.3a) leads to

$$(4.9) \qquad \tau = \frac{R_h^2}{2\gamma n^2}[g_{11} + (g_{21} + \lambda g_{51}d_{12})\bar{W}_1^2$$
$$+ (g_{31} + \lambda g_{51}d_{22})\bar{W}_2^2 - g_{41}\bar{W}_2 - \lambda g_{51}d_{32}\Delta T].$$

Similarly, placing $\bar{W}_0$ and $\bar{N}_{x0}$ from Eq. (4.8) into Eq. (4.3b) gives

$$(4.10) \qquad \bar{W}_1^2 = \frac{1}{d_{13} - d_{23}\bar{W}_2}[d_{33}\bar{W}_2 - d_{43}\bar{W}_2^2 + d_{53}\bar{W}_2^3 + (d_{63} - d_{73}\bar{W}_2)\Delta T]$$

in which coefficients d_{k3} ($k = 1,\ldots,7$) can be found in Eq. (A.5) in Appendix.

Now, introduction of $\bar{W}_1^2$ from Eq. (4.10) into Eq. (4.9) yields the following relation

$$(4.11) \qquad \tau = \frac{R_h^2}{2\gamma n^2}$$
$$\times \left\{ g_{11} + \frac{g_{21} + \lambda g_{51}d_{12}}{d_{13} - d_{23}\bar{W}_2}[d_{33}\bar{W}_2 - d_{43}\bar{W}_2^2 + d_{53}\bar{W}_2^3 + (d_{63} - d_{73}\bar{W}_2)\Delta T]$$
$$+ (g_{31} + \lambda g_{51}d_{22})\bar{W}_2^2 - g_{41}\bar{W}_2 - \lambda g_{51}d_{32}\Delta T \right\}.$$

By setting $\bar{W}_2 \to 0$, we obtain the expression of buckling torsional load as

$$(4.12) \qquad \tau_b = \frac{R_h^2}{2\gamma n^2}\left\{g_{11} + \frac{d_{63}}{d_{13}}(g_{21} + \lambda g_{51}d_{12})\Delta T - \lambda g_{51}d_{32}\Delta T\right\}.$$

The critical buckling torsional load τ_{cr} is obtained by minimizing the buckling load τ_b with respect to the buckling mode (m, n, γ). It is evident from Eq. (4.1a) that maximum deflection of the TSS is

$$(4.13) \qquad W_{\max} = W_0 + W_1 + W_2.$$

Combination of Eqs. (4.8a), (4.10) and (4.13) leads to the following expression of non-dimensional maximum deflection

$$(4.14) \qquad \bar{W}_{\max} = \frac{W_{\max}}{h}$$

$$= \bar{W}_0 + \bar{W}_1 + \bar{W}_2 = \frac{\bar{W}_2}{2} + d_{11}\bar{W}_1^2 + d_{21}\bar{W}_2^2 - d_{31}\Delta T$$

$$+ \frac{1}{\sqrt{d_{13} - d_{23}\bar{W}_2}}[d_{33}\bar{W}_2 - d_{43}\bar{W}_2^2 + d_{53}\bar{W}_2^3 + (d_{63} - d_{73}\bar{W}_2)\Delta T]^{1/2}.$$

Equations (4.11) and (4.14) are used for the load–deflection response analysis of porous FGM TSSs under torsion in a thermal environment. For torsion-loaded shells, the relation between the torsional load and the twist angle is a significant piece of information. The expression of the twist angle is as follows [24]

$$(4.15) \qquad \varphi = \frac{1}{2\pi RL}\int\limits_0^{2\pi R}\int\limits_0^L \left(\frac{\partial u}{\partial y} + \frac{\partial v}{\partial x}\right)dx\,dy.$$

From Eqs. (3.2) and (3.5) it is deduced that

$$(4.16) \qquad \frac{\partial u}{\partial y} + \frac{\partial v}{\partial x} = 2\frac{E_2}{E_1}w_{,xy} - w_{,x}w_{,y} - \frac{2}{E_1}(1+\nu)f_{,xy}.$$

After putting solutions Eqs. (4.1) into Eq. (4.16) and placing the resulting expression into Eq. (4.15), we have

$$(4.17) \qquad \varphi = \left(\frac{\gamma n^2}{4R_h^2}\right)\bar{W}_1^2 + \frac{2}{\bar{E}_1}(1+\nu)\tau$$

$$= \left(\frac{\gamma n^2}{4R_h^2}\right)\frac{g_{22} + \lambda g_{42}(g_{23}\bar{W}_2^2 - G\Delta T)}{g_{12} - (g_{32} + \lambda g_{42}g_{13})\bar{W}_2}\bar{W}_2 + \frac{2}{\bar{E}_1}(1+\nu)\tau.$$

This relation, in combination with Eq. (4.11), is used for the load–rotation response analysis of porous FGM TSSs under torsion in a thermal environment.

5. Results and discussion

Numerical results are presented in this section for simply supported FGM TSSs made of silicon nitride and stainless steel referred to as Si_3N_4 and SUS304, respectively. The properties of constituents are assumed to be nonlinear functions of temperature as [42]

(5.1) $$P = P_0(P_{-1}T^{-1} + 1 + P_1T + P_2T^2 + P_3T^3),$$

where $T = T_0 + \Delta T$ with $T_0 = 300\,\mathrm{K}$ (room temperature) and coefficients P_{-1}, P_0, P_1, P_2 and P_3 are unique for each material. The specific values of these coefficients for Si_3N_4 and SUS304 are given in Table 1. In numerical calculations, the Poisson ratios of constituents and FGM are assumed to be $\nu = 0.28$.

TABLE 1. Temperature-dependent properties of materials, from REDDY and CHIN [43].

Material	Property	P_0	P_{-1}	P_1	P_2	P_3
Si_3N_4	E_c [Pa]	348.43e+9	0	-3.070e-4	2.160e-7	-8.946e-11
	α_c	5.8723e-6	0	9.095e-4	0	0
SUS304	E_m [Pa]	201.04e+9	0	3.079e-4	-6.534e-7	0
	α_m	12.330e-6	0	8.086e-4	0	0

TABLE 2. Comparison of critical buckling torsional loads τ_{cr} [MPa] of very thin Si_3N_4/SUS304 cylindrical shells without porosities and with movable edges $[R/h = 500, L/R = 2, T = 300\,\mathrm{K}]$.

Reference	N^*						
	0	0.2	0.5	1	2	5	10
HUANG *et al.* [27]	74.224	69.044	64.381	60.404	57.139	53.978	51.950
Present **	74.069	68.937	64.296	60.307	56.996	53.714	51.691

**The buckling mode $(m, n, \gamma) = (1, 13, 0.24)$ for $N^* = 0, 0.2, 0.5, 1, 2$ and $(m, n, \gamma) = (1, 12, 0.22)$ for $N^* = 5, 10$.

5.1. Verification

There are no previous studies on torsional stability of FGM TSSs with porosities and elastically restrained edges. Therefore, to verify the proposed work, comparative studies are carried out for special cases of geometry and in-plane boundary conditions. Specifically, a buckling problem of a FGM circular cylindrical shell (CCS) with movable edges and without porosities and surrounding elastic medium (i.e. $a \to \infty$, $\xi = 0$, $c = 0$, $k_1 = k_2 = 0$) is considered. Critical

TABLE 3. Comparison of critical buckling torsional loads τ_{cr} [MPa] of thin Si_3N_4/SUS304 cylindrical shells without porosities and with movable edges [$R/h = 100$, $L^2/Rh = 300$, $T = 300$ K, $(m, n) = (1, 8)$].

Reference	N					
	0	0.2	0.5	1	2	5
SHEN [24]	385.331	426.363	458.291	484.561	507.646	536.192
Present*	385.941	425.199	458.556	487.552	514.525	545.345

*$\gamma = 0.36$ for $N = 0, 0.2, 0.5, 1$ and $\gamma = 0.35$ for $N = 2, 5$.

buckling torsional loads of very thin ($R/h = 500$) and thin ($R/h = 100$) CCSs are computed using Eq. (4.12) and given in Tables 2 and 3 in comparison with result of HUANG *et al.* [27] making use of the Ritz energy method and with result of SHEN [24] using a singular perturbation technique, respectively. In the Table 2, N^* is the volume fraction index for the case of FGM CCS with the ceramic-rich inner surface and metal-rich outer surface, i.e. $V_c = (1/2 + z/h)^{N^*}$. It is evident that a very good agreement is obtained in these comparisons.

In subsequent subsections, numerical results for buckling and postbuckling analyses are presented. In these numerical results, the degree of tangential edge constraint is measured by the non-dimensional tangential stiffness parameter λ defined as Eq. (4.7). Based on this definition, cases of movable ($c = 0$), immovable ($c \to \infty$) and partially movable ($0 < c < \infty$) edges are characterized by values of $\lambda = 0$, $\lambda = 1$ and $0 < \lambda < 1$, respectively. Furthermore, influences of elastic media are evaluated by non-dimensional stiffness parameters K_1, K_2 as defined in Eq. (A.3), in Appendix. For the sake of brevity, TSSs are assumed to be placed at room temperature ($T_0 = 300$ K) and without foundation interaction ($K_1 = K_2 = 0$), unless otherwise specified.

5.2. Buckling analysis

First, the effects of the volume fraction index N, the porosity volume fraction ξ and the type of porosity distribution on critical buckling loads of FGM TSSs with movable edges under torsion are indicated in Table 4. As can be seen, due to an increase in the volume percentage of the ceramic constituent, critical loads are significantly higher when the N index becomes larger. Critical torsional loads are evidently reduced as the porosity volume fraction is increased. Furthermore, the buckling resistance capacity of FGM TSS with evenly distributed porosities is weaker than that of FGM TSS with unevenly distributed porosities. Subsequently, Table 5 and Fig. 3 consider the effects of the geometry ratio L/R, the edge restraint parameter λ and the thermal environment T on the critical buckling loads of FGM TSS with evenly distributed porosities under torsion. It is

clear from Table 5 that critical loads are pronouncedly decreased when the L/R ratio is larger. It is very interesting to note that the tangential constraints of edges have no effect on critical loads at room temperature and have detrimental influence on critical loads at elevated temperatures. Specifically, it is recognized that the critical torsional loads are quickly lowered when edges are more rigorously restrained and environment temperature is more elevated. Obviously, thermally induced compressive forces at restrained edges make the TSS buckle sooner under torsion.

Table 4. Effects of porosities on critical torsional loads τ_{cr}[MPa] of FGM TSSs with movable edges [$R/h = 100$, $L/R = 1.5$, $\lambda = 0$, $T = 300$ K, $R/a = 0.05$, $K_1 = K_2 = 0$, $(m, n) = (1, 9)$]; i, j, k correspond to $\gamma = 0.41, 0.42, 0.43$, respectively.

Porosity	ξ	N				
		0	0.5	1	2	5
Even	0	461.740 (j)	548.598 (j)	583.325 (i)	615.673 (i)	652.620 (i)
	0.1	402.846 (j)	489.239 (j)	523.803 (i)	556.236 (i)	593.483 (i)
	0.2	343.952 (j)	429.752 (j)	464.125 (i)	496.676 (i)	534.296 (i)
	0.3	285.058 (j)	370.077 (j)	404.223 (i)	436.943 (i)	475.039 (i)
Uneven	0	461.740 (j)	548.598 (j)	583.325 (i)	615.673 (i)	652.620 (i)
	0.1	441.262 (j)	527.900 (j)	562.591 (j)	595.024 (i)	632.114 (i)
	0.2	420.784 (j)	507.177 (j)	541.787 (j)	574.315 (j)	611.596 (i)
	0.3	400.286 (k)	486.421 (j)	520.944 (j)	553.526 (j)	590.996 (j)

Table 5. Effects of λ, T and L/R ratio on critical torsional loads τ_{cr}[MPa] of FGM TSSs with evenly distributed porosities [$R/h = 100$, $N = 2$, $\xi = 0.15$, $R/a = 0.05$, $K_1 = K_2 = 0$, $m = 1$]; numbers in parentheses indicate the buckling mode (n, γ).

λ	T [K]	L/R			
		1	1.5	2	2.5
0	300	635.248 (10, 0.49)	526.474 (9, 0.41)	473.007 (8, 0.35)	436.885 (8, 0.34)
	400	623.455 (10, 0.49)	516.685 (9, 0.41)	464.193 (8, 0.35)	428.758 (9, 0.34)
	500	610.183 (10, 0.49)	505.709 (9, 0.41)	454.361 (8, 0.35)	419.656 (8, 0.34)
1	300	635.248 (10, 0.49)	526.474 (9, 0.41)	473.007 (8, 0.35)	436.885 (8, 0.34)
	400	565.926 (10, 0.52)	474.657 (9, 0.44)	431.830 (8, 0.38)	401.386 (8, 0.37)
	500	487.599 (10, 0.56)	414.774 (9, 0.48)	382.388 (9, 0.46)	358.986 (8, 0.40)

Ultimate numerical results in this subsection are shown in Table 6 examining the effects of geometry ratios R/a, R/h and non-dimensional stiffness parameters K_1, K_2 of surrounding elastic media on critical torsional loads of FGM CCSs and TSSs with evenly distributed porosities and partially movable edges ($\lambda = 0.5$) under torsion in a thermal environment ($T = 400$ K). As expected,
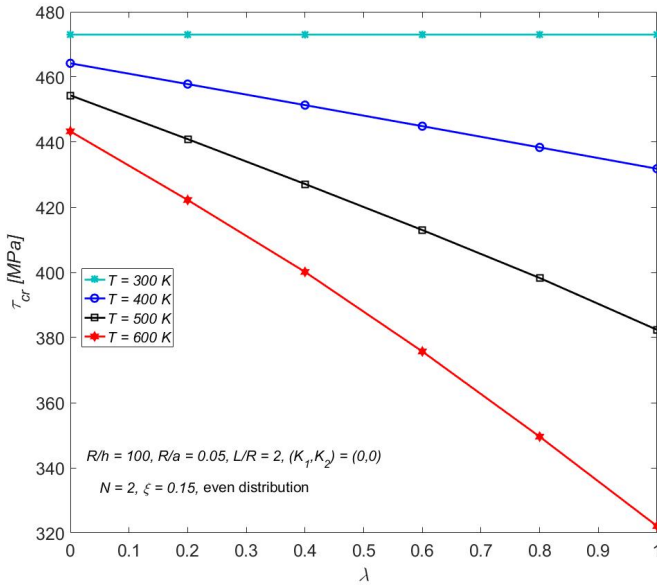
FIG. 3. Effects of tangential edge constraints and thermal environments on critical torsional loads of FGM TSSs with evenly distributed porosities.

buckling resistance capability of FGM TSS become remarkably weaker when the R/h ratio is increased. In contrast, an increase in the ratio of curvature radii R/a leads to obvious increase in critical torsional loads of TSSs. For example, in case of $R/h = 100$ and $(K_1, K_2) = (0, 0)$, the critical torsional load τ_{cr} is

TABLE 6. Effects of geometry and elastic foundation on critical torsional loads τ_{cr} [MPa] of FGM TSSs with evenly distributed porosities [$L/R = 1.5$, $N = 2$, $\xi = 0.15$, $\lambda = 0.5$, $T = 400$, $m = 1$]; numbers in parentheses indicate the buckling mode (n, γ).

R/a	(K_1, K_2)	R/h			
		100	150	200	250
	(0, 0)	439.55 (9, 0.42)	253.75 (10, 0.37)	170.96 (11, 0.35)	125.07 (12, 0.34)
0	(300, 0)	518.44 (9, 0.48)	284.86 (11, 0.44)	186.58 (11, 0.37)	133.49 (12, 0.36)
	(300, 5)	652.36 (10, 0.55)	347.66 (11, 0.48)	223.88 (12, 0.44)	159.05 (13, 0.42)
	(0, 0)	495.71 (9, 0.43)	301.51 (11, 0.42)	210.63 (12, 0.40)	159.78 (13, 0.49)
0.05	(300, 0)	567.42 (10, 0.50)	325.13 (11, 0.44)	222.21 (12, 0.41)	166.11 (13, 0.40)
	(300, 5)	697.94 (10, 0.55)	387.43 (11, 0.48)	258.88 (12, 0.45)	190.18 (13, 0.43)
	(0, 0)	562.25 (9, 0.45)	349.07 (11, 0.44)	250.97 (13, 0.44)	194.35 (14, 0.44)
0.1	(300, 0)	620.24 (10, 0.51)	370.00 (12, 0.48)	259.69 (13, 0.46)	199.14 (14, 0.44)
	(300, 5)	748.93 (10, 0.56)	429.18 (12, 0.52)	294.07 (13, 0.49)	221.52 (14, 0.47)

increased about 28 percent when the R/a ratio increases only 10 percent (from 0 to 0.1). This fact demonstrates that TSSs have the advantage over CCSs in a torsional buckling resistance. Results in Table 6 also indicate that the presence of surrounding elastic media significantly improve the buckling resistance capacity of torsion-loaded FGM TSSs. More specifically, critical loads are obviously enhanced when foundation stiffness parameters, especially the stiffness of Pasternak shear layer, are increased.

5.3. Postbuckling analysis

As a first example of this subsection, the effects of the porosity volume fraction ξ on the postbuckling behavior of FGM TSSs with evenly distributed porosities and movable edges ($\lambda = 0$) under torsion are depicted in Figs. 4 and 5 for load–deflection and load–rotation responses, respectively. As can be observed, the existence of porosity has negative influence on the postbuckling behavior of torsion–loaded FGM TSSs. Both the postbuckling deflection and the twist angle of the shell are considerably increased due to an increase in the volume fraction of porosity. Nevertheless, it is realized that intensity of the snap-through response in the postbuckling region of the TSS is reduced when the volume percentage of porosity is higher. It seems that the presence of pores renders the
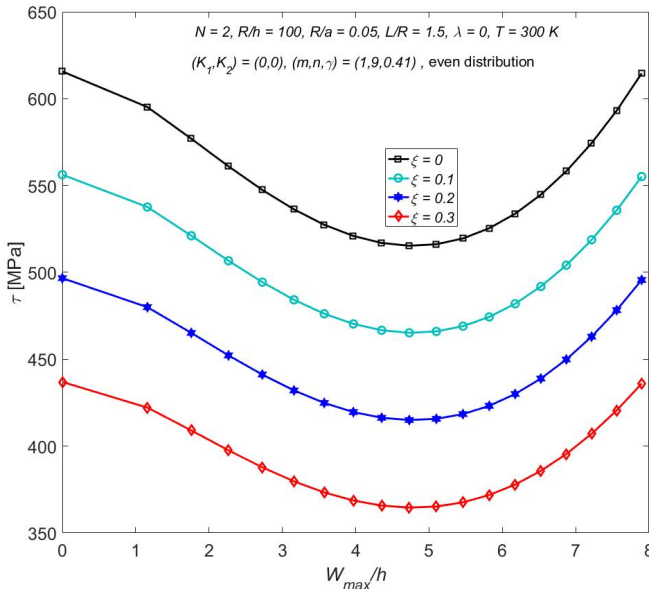

FIG. 4. Effects of porosity volume fraction on torsional load–deflection response of FGM TSSs with evenly distributed porosities under torsion.
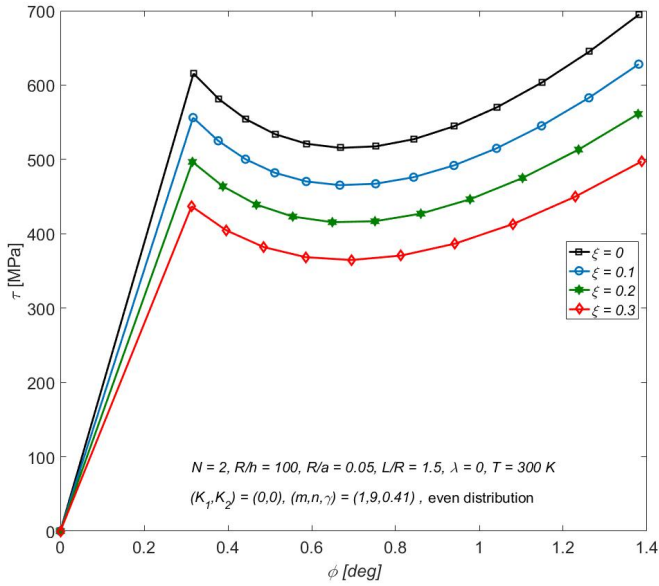
FIG. 5. Effects of porosity volume fraction on torsional load–rotation response of FGM TSSs with evenly distributed porosities under torsion.
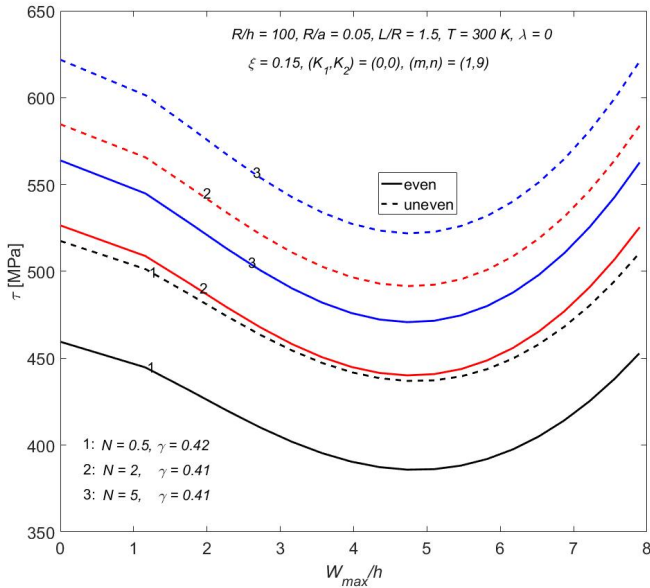

FIG. 6. Effects of volume fraction index and type of porosity distribution on torsional postbuckling curves of FGM TSSs with movable edges.
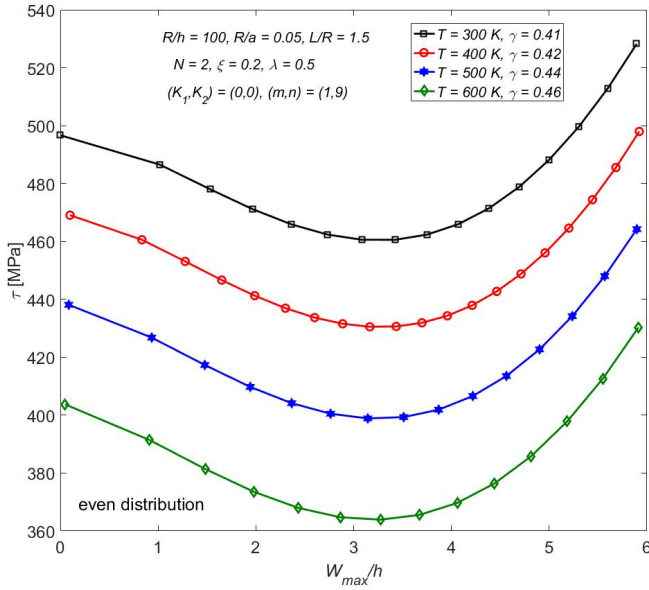
FIG. 7. Effects of thermal environments on torsional load–deflection response of FGM TSSs with partially movable edges and evenly distributed porosities.
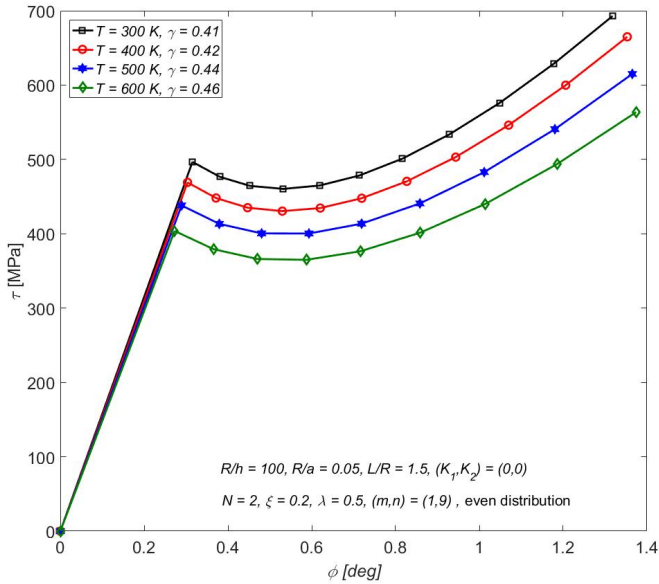

FIG. 8. Effects of thermal environments on torsional load–rotation response of FGM TSSs with partially movable edges and evenly distributed porosities.

FGM softer, buckling resistance capacity of TSS weaker and snapping jump more benign. Next, the effects of the volume fraction index N and the type of porosity distribution on the postbuckling load–deflection response of FGM TSSs with movable edges under the torsional load are examined in Fig. 6. Evidently, the equilibrium path is higher when the N index is larger and/or porosities are unevenly distributed in the FGM shell. It is also recognized that the snap-through response is more intense when the volume percentage of the ceramic constituent is higher.

Next examples are shown in Figs. 7 and 8 considering the effects of environment temperature T on the postbuckling load–deflection and load–rotation responses of FGM TSSs with evenly distributed porosities and partially movable edges ($\lambda = 0.5$) under torsion, respectively. Obviously, when edges are restrained, the enhancement of temperature T leads to substantial decrease in load carrying capability of torsion-loaded FGM TSSs. In contrast, Figs. 7 and 8 demonstrate that the twist angle becomes larger with higher values of environment temperature. Subsequently, the effects of the ratio of curvature radii R/a on the postbuckling behavior of porous FGM TSSs with movable edges surrounded by the Pasternak elastic foundation ($K_1 = 100$, $K_2 = 1$) and subjected to torsion are analyzed in Figs. 9 and 10 for load–deflection and load–rotation responses, respectively. It is clear that critical buckling loads and initial postbuckling equilibrium paths are considerably enhanced as the R/a ratio is increased. However, the intensity of the snap-through response is also increased when the TSS becomes more curved in the meridional direction. In another expression, the buckling resistance capacity of the TSS is stronger while the snap-through response in the postbuckling region is more intense in comparison with CCS ($R/a = 0$).

In the next numerical results, Figs. 11 and 12, plotted with five different values of the parameter λ, show the effects of tangential edge constraints on the postbuckling behavior of FGM TSSs with unevenly distributed porosities surrounded by the Winkler elastic foundation ($K_1 = 200$, $K_2 = 0$) under a torsional load at room temperature. As can be seen, the tangential constraints of boundary edges have pronouncedly beneficial influences on the postbuckling load carrying capability of FGM TSSs at reference temperature. Specifically, although buckling loads are unchanged, postbuckling equilibrium paths are significantly higher and more stable when edges are more severely restrained. This fact suggests that harmful snap-through instability in the postbuckling region of torsionally loaded porous TSSs can be avoided by restraining edges from the tangential displacement. In another situation, effects of tangential edge constraints on the postbuckling behavior of FGM TSSs with unevenly distributed porosities subjected to torsion at elevated temperature ($T = 500\,\mathrm{K}$) are analyzed in Figs. 13 and 14 for load–deflection and load–rotation responses, respectively. As
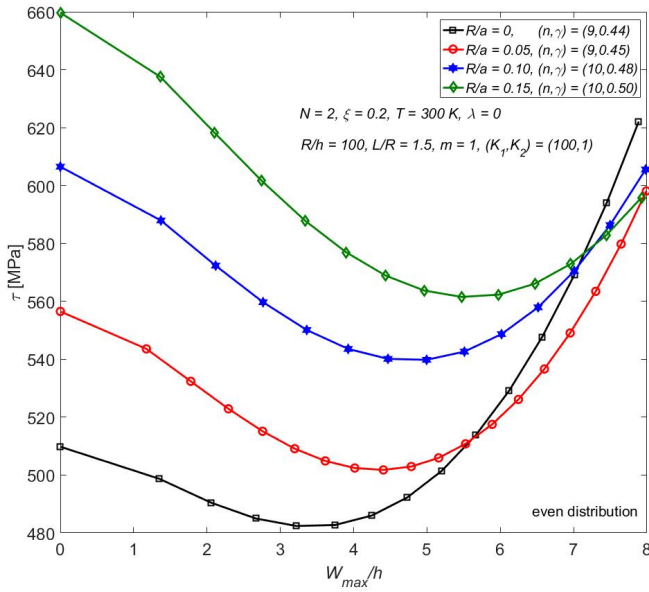
Fig. 9. Effects of R/a ratio on torsional load–deflection response of FGM TSSs with evenly distributed porosities and movable edges.
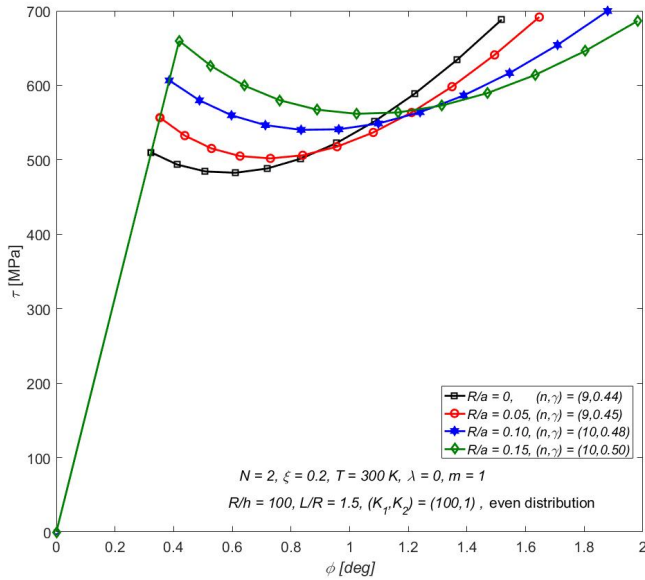

Fig. 10. Effects of R/a ratio on torsional load–rotation response of FGM TSSs with evenly distributed porosities and movable edges.
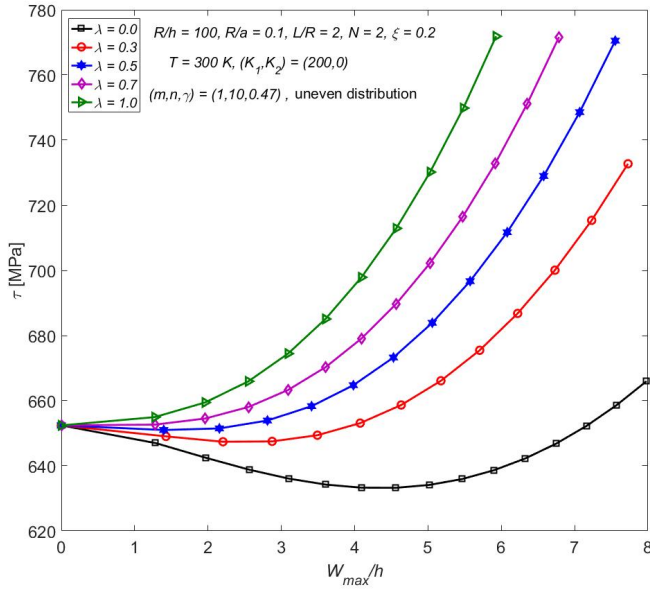
FIG. 11. Effects of tangential edge constraints on torsional load–deflection response of FGM TSSs with unevenly distributed porosities at reference temperature.
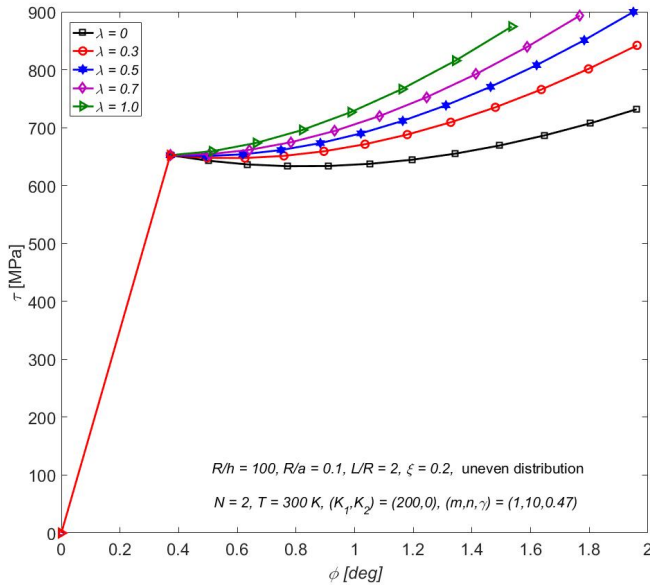

FIG. 12. Effects of tangential edge constraints on torsional load–rotation response of FGM TSSs with unevenly distributed porosities at reference temperature.
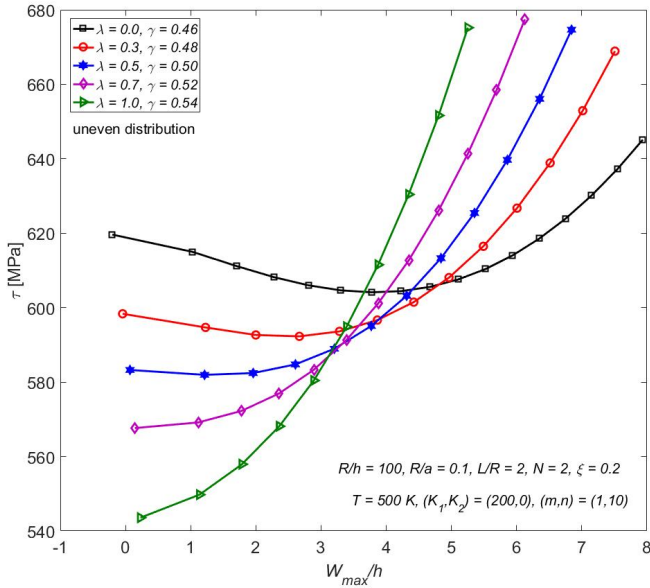
Fig. 13. Effects of tangential edge constraints on torsional load–deflection response of FGM TSSs with unevenly distributed porosities at elevated temperature.
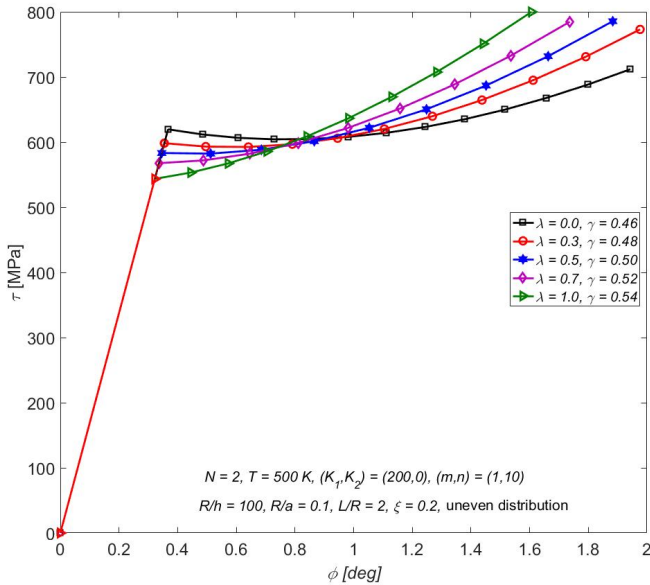

Fig. 14. Effects of tangential edge constraints on torsional load–rotation response of FGM TSSs with unevenly distributed porosities at elevated temperature.
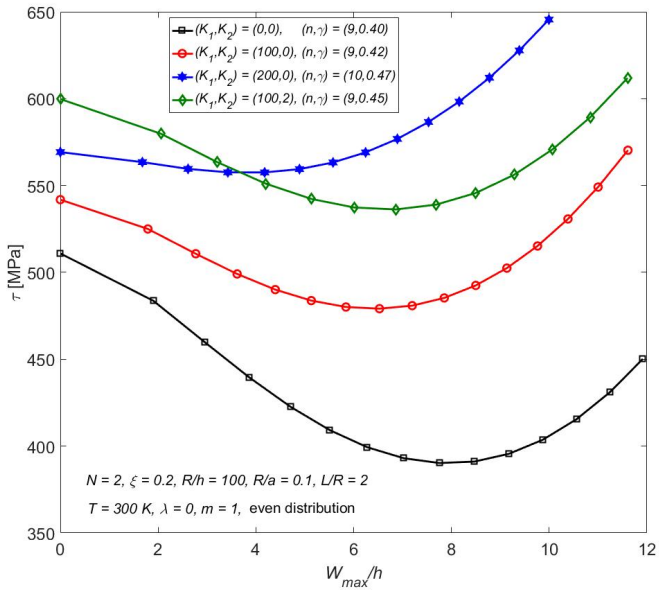
FIG. 15. Effects of elastic media on torsional load–deflection response of FGM TSSs with evenly distributed porosities and movable edges.
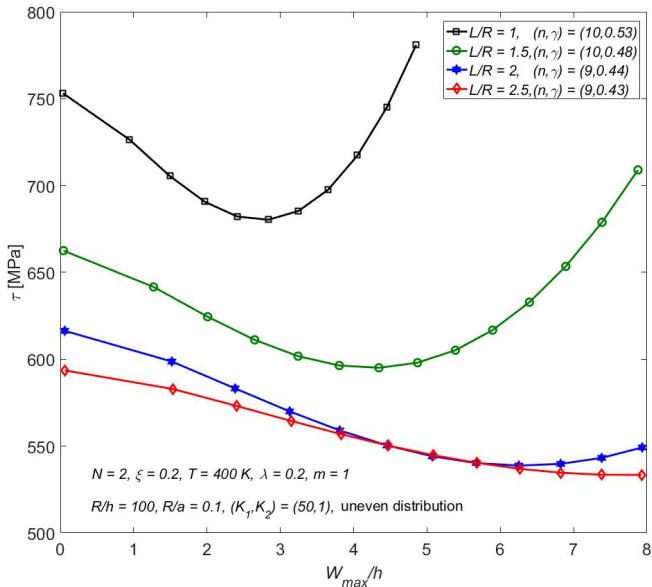

FIG. 16. Effects of length-to-radius ratio on torsional load–deflection response of FGM TSSs with unevenly distributed porosities and partially movable edges.

can be observed, unlike a case of reference temperature, buckling loads and initial postbuckling equilibrium paths of TSSs are remarkably lowered when the λ parameter is increased. Nevertheless, tangential constraints of edges still yield positive effects on the load bearing capability of porous TSSs at deep region of the deflection. Concretely, when the deflection exceeds a definite value, the postbuckling strength of the porous TSS is higher when the edges are more rigorously restrained. It is also found from Figs. 13 and 14 that the twist angle is substantially larger as the restraint stiffness parameter λ is increased. It may be explained that thermally induced compressive forces at restrained edges render the overall rigidity of the TSS reduced and, as a result, the torque resistance capability is weaker.

The influences of surrounding elastic media on the torsional postbuckling behavior of porous FGM TSSs with movable edges are illustrated in Fig. 15. Generally, elastic foundations beneficially influence the buckling resistance capacity and postbuckling load carrying capability of porous FGM TSSs. More concretely, it seems that the Winkler-type foundation improves the stability in the postbuckling region of the TSS and alleviates the intensity of the snapthrough phenomenon, whereas the Pasternak shear layer enhances the buckling resistance capability of the porous FGM TSSs under torsion. Finally, the effects of the L/R ratio on the postbuckling behavior of porous FGM TSSs with almost movable edges ($\lambda = 0.2$), exposed to a thermal environment ($T = 400\,\mathrm{K}$), surrounded by the Pasternak foundation ($K_1 = 50$, $K_2 = 1$) and subjected to torsional load are examined in Fig. 16. As shown, the behavior tendency of the TSS is significantly changed due to variation of the L/R ratio. Specifically, buckling loads and postbuckling paths are rapidly dropped when the L/R ratio is increased from 1 to 1.5 and then are gradually lowered as the L/R ratio varies from 1.5 to 2.5. Moreover, it is recognized that the snap-through response is more intense when the TSS becomes longer.

6. Concluding remarks

The buckling and postbuckling behaviors of FGM TSSs with porosities, surrounding elastic media and tangentially restrained edges subjected to torsion in a thermal environment have been investigated. The combined influences of porosity, tangential edge constraints, elevated temperature and surrounding elastic media on the nonlinear stability of torsionally loaded FGM TSSs have been analyzed. From the above results, the following remarks are reached:

(i) Critical loads and postbuckling equilibrium paths of torsionlly loaded FGM TSSs are significantly dropped due to the presence of pores. However, the severity of the unexpected snap-through phenomenon is more benign when the porosity volume fraction is increased.

(ii) Critical torsional loads are unchanged and considerably decreased when the edges are tangentially restrained at reference and elevated temperatures, respectively.

(iii) Tangential edge constraints have beneficial influences on the postbuckling behavior of torsion-loaded porous FGM TSSs at reference temperature. Specifically, postbuckling load–deflection and load–rotation curves are considerably enhanced while the intensity of the snap-though response is pronouncedly reduced when edges are more rigorously restrained.

(iv) In general, surrounding elastic media beneficially influence the nonlinear stability of torsion-loaded porous FGM TSSs. In particular, the Pasternak shear layer and the Winkler elastic layer render the buckling torsional load larger and the snap-through response in the postbuckling region more benign, respectively.

Appendix

The coefficients g_{i1} $(i = 1, \ldots, 5)$, g_{j2} $(j = 0, \ldots, 4)$ in the Eq. (4.3) are the following:

$$
\begin{aligned}
g_{11} =\ & \bar{D}\left[\frac{m^4\pi^4}{R_h^4 L_R^4} + 6m^2 n^2 \frac{\gamma^2 \pi^2}{R_h^4 L_R^2} + \frac{n^4}{R_h^4}(\gamma^4 + 1) + 2\frac{n^2}{R_h^2}\left(\frac{m^2\pi^2}{R_h^2 L_R^2} + \gamma^2 \frac{n^2}{R_h^2}\right)\right] \\
& + \frac{\bar{E}_1}{2R_h^2}\left\{\left[\frac{n^2 L_R^2 R_a + (m\pi + \gamma n L_R)^2}{n^2 L_R^2 + (m\pi + \gamma n L_R)^2}\right]^2\right. \\
& \left. + \left[\frac{n^2 L_R^2 R_a + (m\pi - \gamma n L_R)^2}{n^2 L_R^2 + (m\pi - \gamma n L_R)^2}\right]^2\right\} \\
& + K_1 \frac{E_m^0}{R_h^4} + K_2 \frac{E_m^0}{R_h^2}\left(\frac{m^2\pi^2}{R_h^2 L_R^2} + \frac{n^2}{R_h^2} + \gamma^2 \frac{n^2}{R_h^2}\right),
\end{aligned}
$$

(A.1)
$$
g_{21} = \frac{m^4\pi^4 + \left(1+\gamma^2\right)^2 n^4 L_R^4}{16(1+\gamma^2)^2 R_h^4 L_R^4}\bar{E}_1, \qquad g_{51} = \left(\frac{m\pi}{R_h L_R}\right)^2 + \left(\gamma \frac{n}{R_h}\right)^2,
$$

$$
\begin{aligned}
g_{31} =\ & \frac{\bar{E}_1}{2R_h^4}(mn\pi)^4\left\{\frac{1}{[(m\pi - \gamma n L_R)^2 + n^2 L_R^2]^2} + \frac{1}{[(m\pi + \gamma n L_R)^2 + n^2 L_R^2]^2}\right. \\
& \left. + \frac{1}{[(3m\pi + \gamma n L_R)^2 + n^2 L_R^2]^2} + \frac{1}{[(3m\pi - \gamma n L_R)^2 + n^2 L_R^2]^2}\right\},
\end{aligned}
$$

$$
\begin{aligned}
g_{41} =\ & \bar{E}_1 \frac{m^2 n^2 \pi^2}{R_h^3}\left\{\frac{1}{4m^2\pi^2} + \frac{(m\pi - \gamma n L_R)^2 + n^2 L_R^2 R_a}{[(m\pi - \gamma n L_R)^2 + n^2 L_R^2]^2}\right. \\
& \left. + \frac{(m\pi + \gamma n L_R)^2 + n^2 L_R^2 R_a}{[(m\pi + \gamma n L_R)^2 + n^2 L_R^2]^2}\right\};
\end{aligned}
$$

$$g_{02} = -K_1 \frac{E_m^0}{R_h^4},$$

$$g_{22} = 4\bar{D}\left(\frac{m\pi}{R_h L_R}\right)^4 + \frac{\bar{E}_1}{4R_h^2} + \frac{3E_m^0}{4R_h^4}K_1 + E_m^0\left(\frac{m\pi}{R_h^2 L_R}\right)^2 K_2,$$

$$g_{12} = \bar{E}_1 \frac{m^2 n^2 \pi^2}{4R_h^3}\left\{\frac{1}{4m^2\pi^2} + \frac{(m\pi - \gamma n L_R)^2 + n^2 L_R^2 R_a}{[(m\pi - \gamma n L_R)^2 + n^2 L_R^2]^2}\right.$$

(A.2)
$$\left. + \frac{(m\pi + \gamma n L_R)^2 + n^2 L_R^2 R_a}{[(m\pi + \gamma n L_R)^2 + n^2 L_R^2]^2}\right\},$$

$$g_{32} = \frac{\bar{E}_1}{4R_h^4}(mn\pi)^4\left\{\frac{1}{[(m\pi - \gamma n L_R)^2 + n^2 L_R^2]^2} + \frac{1}{[(m\pi + \gamma n L_R)^2 + n^2 L_R^2]^2}\right.$$

$$\left. + \frac{1}{[(3m\pi + \gamma n L_R)^2 + n^2 L_R^2]^2} + \frac{1}{[(3m\pi - \gamma n L_R)^2 + n^2 L_R^2]^2}\right\},$$

$$g_{42} = \left(\frac{m\pi}{R_h L_R}\right)^2,$$

where

(A.3) $$\bar{E}_1 = \frac{E_1}{h}, \quad \bar{D} = \frac{D}{h^3}, \quad L_R = \frac{L}{R}, \quad (K_1, K_2) = \frac{R^2}{E_m^0 h^3}(k_1 R^2, k_2)$$

in which E_m^0 is value of E_m computed at room temperature $T_0 = 300\,\mathrm{K}$.

The details of coefficients d_{ij} $(i = 1, \ldots, 3, \, j = 1, 2)$ in Eqs. (4.8) are:

$$d_{11} = \frac{8\nu\lambda g_{13} R_h^2 + \bar{E}_1 n^2}{8\bar{E}_1 R_h (1 + \nu\lambda R_a)}, \quad d_{21} = \frac{\nu\lambda g_{23} R_h}{\bar{E}_1(1 + \nu\lambda R_a)},$$

(A.4) $$d_{31} = \frac{(1 + \nu\lambda) R_h}{\bar{E}_1(1 + \nu\lambda R_a)}G,$$

$$d_{12} = g_{13} - \bar{E}_1 d_{11}\frac{R_a}{R_h}, \quad d_{22} = g_{23} - \bar{E}_1 d_{21}\frac{R_a}{R_h}, \quad d_{32} = G - \bar{E}_1 d_{31}\frac{R_a}{R_h}.$$

The coefficients d_{k3} $(k = 1, \ldots, 7)$ in Eq. (4.10) are defined as follows:

$$d_{13} = g_{02}d_{11} + g_{12} + \lambda d_{12}\frac{R_a}{R_h}, \quad d_{23} = g_{32} + \lambda g_{42}d_{12},$$

(A.5) $$d_{33} = \frac{1}{2}g_{02} + g_{22}, \quad d_{43} = g_{02}d_{21} + \lambda d_{22}\frac{R_a}{R_h},$$

$$d_{53} = \lambda g_{42}d_{22}, \quad d_{63} = g_{02}d_{31} + \lambda d_{32}\frac{R_a}{R_h}, \quad d_{73} = \lambda g_{42}d_{32}.$$

Conflict of interest statement

Authors declare that there is no conflict of interest.

References

1. H.S. SHEN, *Postbuckling analysis of axially-loaded functionally graded cylindrical shells in thermal environments*, Composites Science and Technology, **62**, 977–987, 2002.

2. H.S. SHEN, *Postbuckling analysis of pressure-loaded functionally graded cylindrical shells in thermal environments*, Engineering Structures, **25**, 487–497, 2003.

3. Z. WAN, S. LI, *Thermal buckling analysis of functionally graded cylindrical shells*, Applied Mathematics and Mechanics (English edition), **38**, 1059–1070, 2017.

4. H.V. TUNG, *Postbuckling of functionally graded cylindrical shells with tangential edge restraints and temperature-dependent properties*, Acta Mechanica, **225**, 1795–1808, 2014.

5. P.T. HIEU, H.V. TUNG, *Nonlinear buckling behavior of functionally graded material sandwich cylindrical shells with tangentially restrained edges subjected to external pressure and thermal loadings*, Journal of Sandwich Structures and Materials, **23**, 6, 2000–2027, 2021.

6. S. TRABELSI, A. FRIKHA, S. ZGHAL, F. DAMMAK, *A modified FSDT-based four nodes finite shell element for thermal buckling analysis of functionally graded plates and cylindrical shells*, Engineering Structures, **178**, 444–459, 2019.

7. S. TRABELSI, A. FRIKHA, S. ZGHAL, F. DAMMAK, *Thermal post-buckling analysis of functionally graded material structures using a modified FSDT*, International Journal of Mechanical Sciences, **144**, 74–89, 2018.

8. E. BAGHERIZADEH, Y. KIANI, M.R. ESLAMI, *Mechanical buckling of functionally graded material cylindrical shells surrounded by Pasternak elastic foundation*, Composite Structures, **93**, 11, 3063–3071, 2011.

9. H.S. SHEN, *Postbuckling of shear deformable FGM cylindrical shells surrounded by an elastic medium*, International Journal of Mechanical Sciences, **51**, 372–383, 2009.

10. K. FOROUTAN, L. DAI, *Static and dynamic thermal post-buckling analysis of imperfect sigmoid FG cylindrical shells resting on a non-uniform elastic foundation*, European Journal of Mechanics – A/Solids, **97**, 104770, 2023.

11. N. WATTANASAKULPONG, V. UNGBHAKORN, *Linear and nonlinear vibration analysis of elastically restrained ends FGM beams with porosities*, Aerospace Science and Technology, **32**, 111–120, 2014.

12. A. GUPTA, M. TALHA, *Influence of initial geometric imperfections and porosity on the stability of functionally graded material plates*, Mechanics Based Design of Structures and Machines, **46**, 6, 693–711, 2018.

13. P.H. CONG, T.M. CHIEN, N.D. KHOA, N.D. DUC, *Nonlinear thermomechanical buckling and post-buckling response of porous FGM plates using Reddy's HSDT*, Aerospace Science and Technology, **77**, 419–428, 2018.

14. M.C. TRINH, T. MUKHOPADHYAY, S.E. KIM, *A semi-analytical stochastic buckling quantification of porous functionally graded plates*, Aerospace Science and Technology, **105**, 105928, 2020.

15. L.T. CUONG, T.V. LOC, B.Q. TINH, N.X. HOANG, M.A. WAHAB, *Isogeometric analysis for size-dependent nonlinear thermal stability of porous FG microplates*, Composite Structures, **221**, p. 110838, 2019.

16. V.T. Long, H.V. Tung, *Thermal nonlinear buckling of shear deformable functionally graded cylindrical shells with porosities*, AIAA Journal, **59**, 6, 2233–2241, 2021.

17. V.T. Long, H.V. Tung, *Thermomechanical nonlinear buckling of pressurized shear deformable FGM cylindrical shells including porosities and elastically restrained edges*, Journal of Aerospace Engineering, **34**, 3, p. 04021011, 2021.

18. V.T. Long, H.V. Tung, *Postbuckling responses of porous FGM spherical caps and circular plates including edge constraints and nonlinear three-parameter elastic foundations*, Mechanics Based Design of Structures and Machines, 2021, doi: 10.1080/15397734.2021.1956327.

19. A. Tabiei, G.J. Simitses, *Buckling of moderately thick, laminated cylindrical shells under torsion*, AIAA Journal, **32**, 3, 639–647, 1994.

20. Y.S. Kim, G.A. Kardomateas, A. Zureick, *Buckling of thick orthotropic cylindrical shells under torsion*, Journal of Applied Mechanics, **66**, 1, 41–50, 1999.

21. X. Zhang, Q. Han, *Buckling and postbuckling behaviors of imperfect cylindrical shells subjected to torsion*, Thin-Walled Structures, **45**, 1035–1043, 2007.

22. A.M. Najafov, A.H. Sofiyev, N. Kuruoglu, *Torsional vibration and stability of functionally graded orthotropic cylindrical shells on elastic foundations*, Meccanica, **48**, 829–840, 2013.

23. A.H. Sofiyev, N. Kuruoglu, *Torsional vibration and buckling of the cylindrical shell with functionally graded coatings surrounded by an elastic medium*, Composites Part B, **45**, 1133–1142, 2013.

24. H. Shen, *Torsional buckling and postbuckling of FGM cylindrical shells in thermal environments*, International Journal of Non-Linear Mechanics, **44**, 644–657, 2009.

25. H.S. Shen, *Torsional postbuckling of nanotube-reinforced composite cylindrical shells in thermal environments*, Composite Structures, **116**, 477–488, 2014.

26. H. Huang, Q. Han, *Nonlinear buckling of torsion-loaded functionally graded cylindrical shells in thermal environments*, European Journal of Mechanics/A Solids, **29**, 42–48, 2010.

27. H. Huang, Q. Han, N. Feng, X. Fan, *Buckling of functionally graded cylindrical shells under combined loads*, Mechanics of Advanced Materials and Structures, **18**, 5, 337–346, 2011.

28. D.V. Dung, L.K. Hoa, *Research on nonlinear torsional buckling and post-buckling of eccentrically stiffened functionally graded thin circular cylindrical shells*, Composites Part B: Engineering, **51**, 300–309, 2013.

29. D.V. Dung, L.K. Hoa, *Nonlinear torsional buckling and postbuckling of eccentrically stiffened FGM cylindrical shells in thermal environment*, Composites Part B: Engineering, **69**, 378–388, 2015.

30. V.H. Nam, N.T. Phuong, K.V. Minh, P.T. Hieu, *Nonlinear thermo-mechanical buckling and post-buckling of multilayer FGM cylindrical shell reinforced by spiral stiffeners surrounded by elastic foundation subjected to torsional loads*, European Journal of Mechanics/A Solids, **72**, 393–406, 2018.

31. V.H. Nam, N.T. Trung, L.K. Hoa, *Buckling and postbuckling of porous cylindrical shells with functionally graded composite coating under torsion in thermal environment*, Thin-Walled Structures, **144**, p. 106253, 2019.

32. M. Stein, J.A. McElman, *Buckling of segments of toroidal shells*, AIAA Journal, **3**, 9, 1704–1709, 1965.

33. P.A. Cooper, *Buckling of nearly cylindrical shells under lateral pressure*, AIAA Journal, **10**, 2, 232–234, 1971.

34. J.W. Hutchinson, *Initial postbuckling of toroidal shell segments*, International Journal of Solids and Structures, **3**, 1, 97–115, 1967.

35. D.G. Ninh, D.H. Bich, *Nonlinear buckling of eccentrically stiffened functionally graded toroidal shell segments under torsional load surrounded by elastic foundation in thermal environment*, Mechanics Research Communications, **72**, 1–15, 2016.

36. V.T. Long, H.V. Tung, *Mechanical buckling analysis of thick FGM toroidal shell segments with porosities using Reddy's higher order shear deformation theory*, Mechanics of Advanced Materials and Structures, **29**, 27, 5923–5932, 2022.

37. V.T. Long, H.V. Tung, *Buckling behavior of thick porous functionally graded material toroidal shell segments under external pressure and elevated temperature including tangential edge restraint*, Journal of Pressure Vessel Technology, **144**, 5, p. 051310, 2022.

38. P.T. Hieu, H.V. Tung, *Thermomechanical nonlinear buckling of pressure-loaded carbon nanotube reinforced composite toroidal shell segment surrounded by an elastic medium with tangentially restrained edges*, Proceedings of the Institution of Mechanical Engineers, Part C: Journal of Mechanical Engineering Science, **233**, 9, 3193–3207, 2019.

39. P.T. Hieu, H.V. Tung, *Thermal and thermomechanical buckling of shear deformable FG-CNTRC cylindrical shells and toroidal shell segments with tangentially restrained edges*, Archive of Applied Mechanics, **90**, 7, 1529–1546, 2020.

40. L.T.N. Trang, H.V. Tung, *Thermal nonlinear stability of functionally graded porous material nearly cylindrical shells with surrounding elastic media and tangentially restrained edges,* Mathematical Methods in the Applied Sciences, **46**, 7285–7304, 2023.

41. L.T.N. Trang, H.V. Tung, *Postbuckling behavior of functionally graded porous toroidal shell segments with surrounding elastic media subjected to combined mechanical loads*, ZAMM, 2023, doi: 10.1002/zamm.202200257.

42. Y.S. Touloukian, *Thermophysical Properties of High Temperature Solid Materials*, MacMillan, New York, 1967.

43. J.N. Reddy, C.D. Chin, *Thermomechanical analysis of functionally graded cylinders and plates*, Journal of Thermal Stresses, **21**, 593–626, 1998.